

# On stimulating fungi *Pleurotus ostreatus* with hydrocortisone

Mohammad Mahdi Dehshibi<sup>a,\*</sup>, Alessandro Chiolerio<sup>b,c</sup>, Anna Nikolaidou<sup>b,d</sup>, Richard Mayne<sup>b</sup>,  
Antoni Gandia<sup>e,f</sup>, Mona Ashtari<sup>g</sup>, Andrew Adamatzky<sup>b,\*\*</sup>

<sup>a</sup>Department of Computer Science, Universitat Oberta de Catalunya, Barcelona, Spain

<sup>b</sup>Unconventional Computing Laboratory, UWE, Bristol, UK

<sup>c</sup>Center for Sustainable Future Technologies, Istituto Italiano di Tecnologia, Torino, Italy

<sup>d</sup>Department of Architecture, UWE, Bristol, UK

<sup>e</sup>Institute for Plant Molecular and Cell Biology, CSIC-UPV, Valencia, Spain

<sup>f</sup>Mogu S.r.l., Inarzo, Italy

---

## Abstract

Fungi cells can sense extracellular signals via reception, transduction, and response mechanisms, allowing them to communicate with their host and adapt to their environment. They feature effective regulatory protein expressions that enhance and regulate their response and adaptation to various triggers such as stress, hormones, physical stimuli as light, and host factors. In our recent studies, we have shown that *Pleurotus* oyster fungi generate electrical potential impulses in the form of spike events in response to their exposure to environmental, mechanical and chemical triggers, suggesting that the nature of stimuli may be deduced from the fungal electrical responses. In this study, we explored the communication protocols of fungi as reporters of human chemical secretions such as hormones, addressing whether fungi can sense human signals. We exposed *Pleurotus* oyster fungi to hydrocortisone, which was directly applied to the surface of a fungal-colonised hemp shavings substrate, and recorded the electrical activity of the fungi. Hydrocortisone is a medicinal hormone replacement that is similar to the natural stress hormone cortisol. Changes in cortisol levels released by the body indicate the presence of disease and can have a detrimental effect on physiological process regulation. The response of fungi to hydrocortisone was also explored further using X-ray to reveal changes in the fungi tissue, where receiving hydrocortisone by the substrate can inhibit the flow of calcium and, as a result, reduce its physiological changes. This research could open the way for future studies on adaptive fungal wearables capable of detecting human physiological states and biosensors built of living fungi.

*Keywords:* fungi, hydrocortisone, biosensor, electrical activity

---

## 1. Introduction

All living organisms have evolved elaborate communication processes and mechanisms to sense, respond, and adapt to the surrounding environment in order to survive. These processes take place through reception, transduction, and response systems, which enable them to sense and adapt to their surroundings in response to a variety of cues such as nutrients, light, gases, stress, and host

---

\*Corresponding author; Email: mohammad.dehshibi@yahoo.com;mdehshibi@uoc.edu

\*\*Corresponding author; Email: andrew.adamatzky@uwe.ac.uk

factors. Any form of communication requires the existence of three essential elements: a sender, a message, and a receiver. The process begins with a sender releasing a message and ends with a receiver understanding the message [1]. Fungi are composed of eukaryotic cells that report, react, and adapt to external stimuli primarily through signal transduction pathways [2]. They have extracellular and intracellular sensing mechanisms, as well as protein receptors that enable them to detect and respond to a variety of signals. *Pleurotus ostreatus*, a basidiomycete fungi, has effective regulatory protein expression that enhances its adaptation to stress triggers [3].

In our previous studies, we reported that the oyster fungi *Pleurotus djamor* exhibit trains of electrical potential spikes similar to action potential spikes [4, 5, 6, 7]. Our initial assumption was that spike trains might reflect increasing mycelium propagation in the substrate, nutrient and metabolite transport, and communication processes within the mycelium network. We investigated the information-theoretic complexity of fungal electrical activity [8, 9, 10] to pave the way for additional investigation into sensorial fusion and fungi decision making [11, 12, 13]. Later, in a series of laboratory experiments [14, 15], we demonstrated that fungal electrical activity patterns, specifically mycelium bound hemp composite, changes in response to stimuli such as light, mechanical stretching, and attractants and repellents. Our findings demonstrated that fungi are a promising candidate for producing sustainable textiles for use as eco-friendly bio-wearables.

We present an illustrative scoping study in which we investigate the short and long-term dynamics in mycelium of the oyster fungi *Pleurotus ostreatus* in response to stimulation with hydrocortisone. The purpose of this study is to enthuse the scientific community to address the issue of fungi being able to sense animal hormones. The human body's adrenal glands release hormones such as cortisol and adrenaline. Cortisol levels in various bodily fluids can range from 4 pM to 70 pM [16, 17]. Sweat cortisol levels have a strong correlation with salivary cortisol concentrations [18], and the optimal cortisol level ranges from 0.02 to 0.5 M [16, 17]. Monitoring cortisol levels in bodily fluids, which can be altered by chronic stress and disease, is critical for maintaining healthy physiological conditions. For this study, not only are the electrical activities investigated, but the substrate is also irradiated with the X-ray beam from multiple angles to produce cross-sectional images of the substrate [19]. This multimodal approach enables us to identify and track the dynamics of changes in the tissue of the mycelium anatomy.

We demonstrated that fungi's electrical responses and reconstructed computed tomography images can be used to detect the presence of stimuli. The findings could lead to the development of biosensing patches for use in organic electronics and bio-electronics, especially with living substrates, which offer a great opportunity to integrate natural systems' parallel sensing and information processing capabilities into future and emerging wearables.

The rest of this paper is structured as follows. Section 2 presents the experimental setup and details of the analysis. Experimental results are discussed in Section 3. The discussion is given in Section 4. Finally, the paper is concluded in Section 5.

## 2. Methods

### 2.1. Experimental setup

A commercial strain of the fungus *Pleurotus ostreatus* (Mogu's collection code 21-18), preselected for showing a superior fitness growing on different lignocellulosic substrates, was cultured on sterilised hemp shives contained in plastic boxes c.  $35 \times 20 \text{ cm}^2$  in darkness at ambient room temperature c.  $22^\circ \text{C}$ . Particles of substrate well colonised by the fungus were spread on rectangular fragments, c.  $12 \times 12 \text{ cm}^2$ , of moisturised nonwoven hemp fibre mats. When the mats were properly

colonised, as visually confirmed by white and homogeneous mycelial growth on the surface, these were used in the experiments. The humidity of the hemp mats ranged from 70% to 80% (Merlin-Laser Protimeter, UK). The experiments were carried out in a room with an ambient temperature of c. 21 °C in the absence of light. It is worth mentioning that it takes approximately 25 days for the mats to be properly colonised, depending on the mat size, the ambient room temperature, and the lignocellulosic substrates chosen for the experiments. Figure 1 shows examples of the experimental setups.



Figure 1: Experimental setup. (a) Exemplar locations of electrodes. (b) Electrode pairs and logging setup in the tent.

Electrical activity of the colonised hemp mats was recorded using pairs of iridium-coated stainless steel sub-dermal needle electrodes (Spes Medica S.r.l., Italy) with twisted cables, via a high-resolution data logger with a 24-bit A/D converter, galvanic isolation, and software-selectable sample rates (Pico Technology, UK). The electrodes were placed in a straight line with a distance of 1-2 cm. To keep the electrodes stable, we put a polyurethane pad underneath the fabric. As a result, the electrode pairs were inserted through the fabric and onto the polyurethane pad, as shown in Fig. 1(a).

In each trial, we recorded the electrical activity of seven electrode pairs simultaneously. Each pair of electrodes, referred to as a Channel (Ch), reported a difference in the electrical potential between the electrodes. The electrical activity was recorded at a rate of one sample per second (1 Hz), with logging times ranging from 60.04 to 93.45 hours for the different experiments. Throughout the recording, the logger took as many samples as it could (typically up to 600 per second) and saved the average value. We set the acquisition voltage range to 156 mV with an offset accuracy of 9  $\mu$ V at 1 Hz to maintain a gain error of 0.1%. Each electrode pair was considered independently with a noise-free resolution of 17 bits and conversion time of 60 ms. We measured and logged a range of resistances 1-1.6 k $\Omega$  using Fluke 8846A precision multi-meter, where the test current being  $1 \pm 0.0013 \mu$ A, once per 10 seconds,  $5 \times 10^4$  samples per trial [7]. Furthermore, the electrical resistance of the electrodes is always less than 10  $\Omega$ , making it minor in comparison to the resistance of the mycelium. Even employing pure gold electrodes would have no effect on the trials. Figure 1(b) shows one of the recording setup inside a light-proof growing tent.

For stimulation, we used hydrocortisone (Solu-Cortef trademark, 4 mL Act-O-Vial, Pfizer, Athens, Greece). We then applied 2 mL of the resulting solution to the surface of the colonised substrate in the loci surrounding Ch4 and Ch5.

The following was the rationale behind the dosage selection: human patients weighing 80 kg are typically given 20 mg of synthetic cortisol per day for a variety of diseases, such as maintenance therapy for patients with hypopituitarism. As a result, 20 mg divided by 80 kg yields 0.25 mg/kg.

Hemp mats colonised with fungi weighed around 100-200 g each, so a 2 mL dose of 250  $\mu\text{g}$  was needed.

## 2.2. Electrical Activity Analysis

Extracellular signals which surpassed a certain amplitude threshold with depolarisation, repolarisation, and refractory cycles are referred to as spike events (see Fig. 2). Spike events represent the physiological and morphological processes of mycelium in the colonised hemp mat. We proposed a novel method for identifying spiking events, including three main stages as (1) splitting signal into chunks, (2) smoothing the chunk by mapping the constant amplitude to an instantaneous amplitude, and (3) detecting spike events.

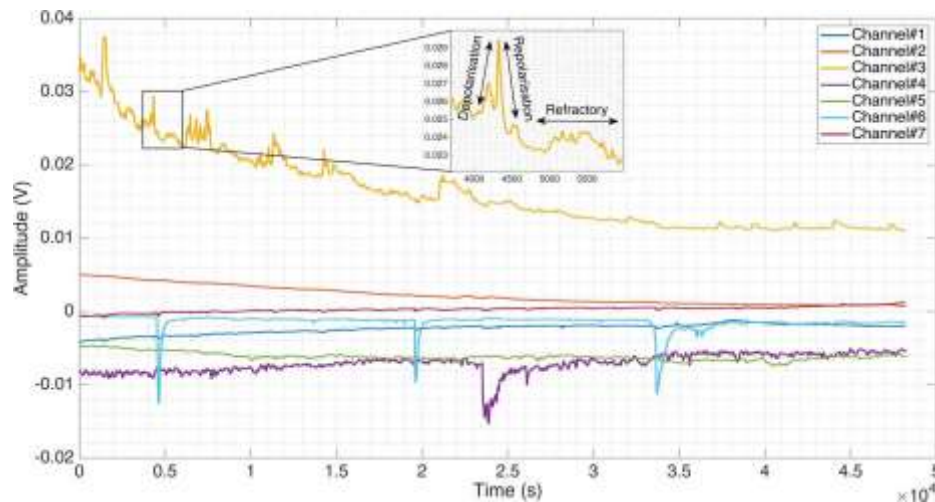


Figure 2: An example of electrical activity observed in seven channels of colonised hemp mats with fungi over 13.3 hours. The inserts are zoomed in on one channel to display a spike event with ‘depolarisation’, ‘repolarisation’, and ‘refractory’ cycles. This spike has a duration of 2258 seconds and a refractory time of 1426 seconds. The rates of depolarisation and repolarisation are 54.85 and 45.75  $\mu\text{V}/\text{s}$ , respectively.

Assume  $X = \{(t_i, x_i)\}_{i=1}^C$  is a recording set of  $C$  channels with the entire length of  $T$  seconds and samplings rate of  $f_s$  Hz, where  $x$  defines the signal’s sample value at time  $t$ ,  $1 \leq t \leq T$ . Our objective is to detect the set of spike events  $S = \{s_1, s_2, \dots, s_\eta\}$  where  $\eta \ll T$ . We segmented the signal  $X$  using the idea of the variable size sliding window to analyse its dynamics before and after hydrocortisone application in the same intervals. Each segment was then subdivided into chunks of  $m = \{1, 2, 4, 8, 16\}$  hours. Note that the chunk  $m = 16$  in all 16 experiments does not have the same length that resulted in 12 to 16 hours of electrical activity recording.

The electrical activity of the colonised hemp mats with fungi displays diffraction patterns. The presence of these diffraction patterns from multiple slits can cause determining spike events to be distorted. The envelope of an oscillating signal can expand the concept of constant amplitude to instantaneous amplitude and, therefore, bypass multiple slits with a single slit diffraction pattern to outline significant extremes, i.e., spike events [10].

To obtain the signal envelope ( $\xi$ ), we used the discrete Fourier Transform, as implemented in the Hilbert transform, to detect the analytical signal. Then, inspired by Marple et al. [20], we set the negative frequency in half of each spectral period to zero, resulting in a periodic one-sided

spectrum. More formally, using the sampling theorem [21], we convert the input chunk<sup>1</sup>,  $X$ , into a sequence of values with the sample period of  $\tau = \frac{1}{f_s}$  (see Eq. 1).

$$L[n] = \tau \cdot x(n\tau), \quad 0 \leq n \leq N - 1 \quad (1)$$

where  $N$  is an even number corresponding to the number of discrete-time analytical signal points. To obtain the  $N$ -point one-sided discrete-time analytic signal using Hilbert transform [20], we need to calculate the discrete-time Fourier transform of  $L[n]$ , with sampling at  $\tau$  intervals to prevent aliasing (see Eq. 2). We take the second numerical signal derivation ( $L = \frac{\partial^2 X}{4\partial t^2}$ ) to highlight effective signal peaks and neutralise diffraction patterns.

$$F(\omega) = \tau \sum_{n=0}^{N-1} L[n] e^{-i2\pi\omega\tau n} \quad (2)$$

where  $|\omega| \leq \frac{1}{2\tau}$  Hz. To obtain a periodic one-sided spectrum ( $Z[k]$ ), we set the negative frequency in half of each spectral period to zero and calculate the spectrum using Eq. 3.

$$Z[k] = \begin{cases} F[0], & \text{for } k = 0 \\ 2F[k], & \text{for } 1 \leq k \leq \frac{N}{2} - 1 \\ F[\frac{N}{2}], & \text{for } k = \frac{N}{2} \\ 0, & \text{for } \frac{N}{2} + 1 \leq k \leq N - 1. \end{cases} \quad (3)$$

To obtain the envelope of the original signal  $x(t)$ , we need to calculate the inverse discrete-time Fourier transform of  $F(\omega)$  and  $Z[k]$  (see Eq. 4).

$$x_a[n] = F^{-1}[F(\omega)], \quad z_a[n] = F^{-1}[Z[k]]. \quad (4)$$

where  $F^{-1}[\cdot]$  takes the inverse of the Fourier transform,  $x_a$  and  $z_a$  are the analytical signals, and  $z_a[n] = \frac{1}{N\tau} \sum_{k=0}^{N-1} Z[k] e^{\frac{2\pi i k n}{N}}$ . By taking the root-mean-square value of the analytical signals as in Eq. 5, we can calculate  $\xi$  for the signal  $X$ .

$$\begin{aligned} e_a[n] &= x_a[n] + jz_a[n], \\ \xi[n] &= \sqrt{e_a[n] \times \bar{e}_a[n]}. \end{aligned} \quad (5)$$

where  $\bar{e}_a$  is the the complex conjugate of  $e_a$ , and  $j$  refers to the imaginary part of the analytical signal. We construct an intermediate representation ( $\tilde{x}$ ) of the input signal using the upper and lower envelopes to identify spike events. All amplitude values greater than or equal to the upper envelope and less than or equal to the lower envelope are replaced with the upper and lower envelope values, respectively, while all other amplitude values are preserved. Then, as in Eq. 6, we calculate the absolute differences between the input signal ( $x$ ) and this intermediate representation ( $\tilde{x}$ ).

---

<sup>1</sup>Note that here we intentionally drop the  $m$  superscript to simplify mathematical notations.

$$\tilde{x}[n] = \begin{cases} \xi_l[n], & x[n] \leq \xi_l[n] \\ \xi_u[n], & x[n] \geq \xi_u[n] \\ x[n], & \text{otherwise.} \end{cases}$$

$$\Phi[n] = |x[n] - \tilde{x}[n]|. \quad (6)$$

where  $\xi_l$  and  $\xi_u$  are the lower and upper envelopes, respectively. We locate all local maxima (peaks) of the  $\Phi[n]$  where the minimum peak prominence is  $\gamma$ . Here,  $\gamma$  is the 99% of confidence interval calculating using Eq. 7.

$$\gamma = \bar{\Phi}[n] + z^* \sqrt{\frac{\sigma}{N}}. \quad (7)$$

where  $z^* = 2.576$  [22], and  $\bar{\Phi}[n]$  and  $\sigma$  are the mean and standard deviation of  $\Phi[n]$ . The proposed spike detection algorithm has true-positive and false-positive rates of 76% and 16%, respectively, implying that we missed 20% of the spike events. However, because this limitation applies to all trials, we report the amortised complexity analysis. Figure 3 shows an example of the proposed method's results.

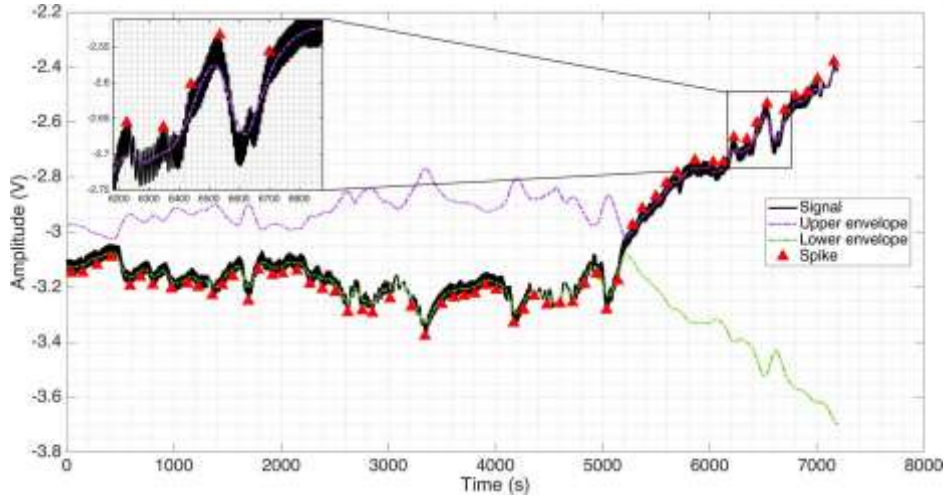


Figure 3: Construct the intermediate representation of an input signal using Eq. 6, where the upper and lower envelopes are shown in violet and green dash lines, respectively. We zoomed in on one chunk electrical activity to highlight the identified spike events.

### 2.3. CT Images Analysis

To gain a better understanding of the effect of stimuli on the fungal substrate, we prepared two containers. Two hours before being irradiated with an X-Ray beam using the dual-energy Discovery City 750 HD CT scanner, one container received no stimuli, while the other received hydrocortisone. The detector provides for data acquisition with 64 detector rows of 0.625 mm collimation. Together

with a z-flying focal spot, this allows simultaneous acquisition of data in  $64 \times 0.625$  slices. The tubes were operated at 120 kVp. The gantry rotation time of the system is 0.35 seconds. CT images were reconstructed using Adaptive Statistical Iterative Reconstruction [23]. The image sets were reconstructed at a slice thickness of 1.25 mm, performing 128 slices per rotation (see Fig. 4(a)). We used two different containers since the fungal colony retains its integrity through the flow of cytoplasm in the mycelium network, where calcium waves [24] and associated electrical potential waves change the propagation coordinate of this flow.

Therefore, we were able to analyse the stimuli spread across the flow of cytoplasm by comparing the CT image of the container that had not received any stimulus with the container that had only one segment exposed (see Figs. 4(b)–4(c)). When working with images in the spatial domain, we deal with changes in pixel values with respect to the scene. In the frequency domain, however, we are interested in the rate at which the pixel values in the spatial domain change, which provides us with a better understanding of the underlying distribution of changes and complexities. The discrete cosine transform (DCT) was used in this study (see Eq.8) to transform the input CT image  $I_{R \times C}$  from the spatial domain to the frequency domain, allowing us to divide the image into spectral sub-bands of varying significance. This transform can also concentrate the majority of the image's visually important details in just a few DCT coefficients. This property enables us to uncover changes in the substrate that are not apparent throughout visual inspection.

$$DCT_{pq} = \alpha_p \alpha_q \sum_{r=0}^{R-1} \sum_{c=0}^{C-1} I_{rc} \cos \frac{\pi(2r+1)p}{2R} \cos \frac{\pi(2c+1)q}{2C},$$

$$\alpha_p = \begin{cases} 1/\sqrt{R} & p=0 \\ 1/(2\sqrt{R}) & 1 \leq p \leq R-1 \end{cases} \quad \alpha_q = \begin{cases} 1/\sqrt{C} & q=0 \\ 1/(2\sqrt{C}) & 1 \leq q \leq C-1 \end{cases} . \quad (8)$$

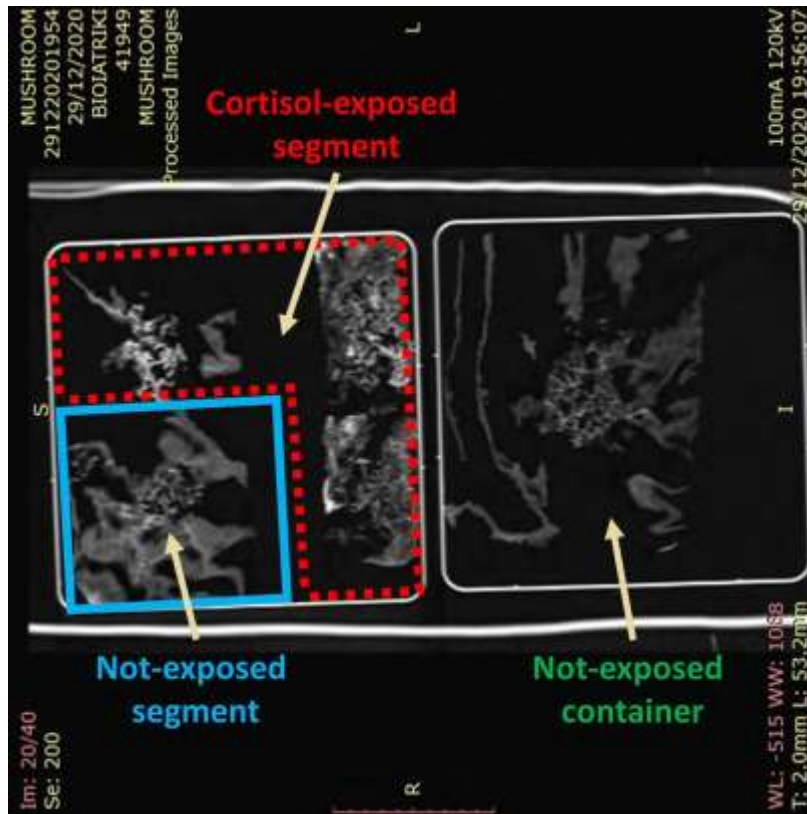
where  $DCT_{pq}$  is the DCT coefficient in row  $p$  and column  $q$  of the DCT matrix,  $I_{R \times C}$ , is the intensity of the pixel in row  $R$  and column  $C$ . Figure 5 shows three examples of the results obtained by applying DCT to CT images.

#### 2.4. Statistical and Information Theory Metrics

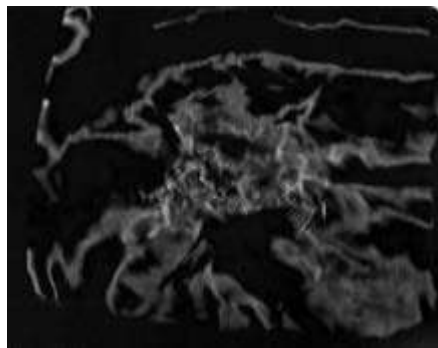
In statistics [25] and information theory [26], the concept of entropy is essential. In statistics, entropy refers to the inference functional for an updating process, and in information theory, it specifies the shortest attainable encoding scheme. Recent advances in complex dynamical systems, on the other hand, have necessitated an extension of the entropy theory beyond the conventional Shannon-Gibbs entropy ( $H$ ) [27]. In this study, we used the Rényi ( $R_q$ ) [28] and Tsallis ( $T_q$ ) [29] additive entropy concepts, which are generalisations of the classical Shannon entropy. Regardless of the generalisation, these two entropy measurements are used in conjunction with the Principle of maximum entropy, with entropy's main application being in statistical estimation theory. Shannon, Tsallis, and Rényi entropy measurements are expressed as in Eq. 9.

$$H(S) = - \sum_i p(s_i) \log p(s_i),$$

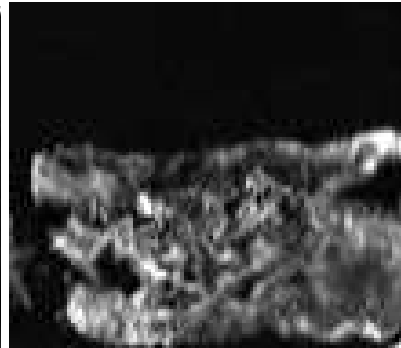
$$T_q(p_i) = \frac{k}{q-1} \left( 1 - \sum_i p_i^q \right), \quad R_q(S) = \frac{1}{1-q} \log \sum_i p_i^q . \quad (9)$$



(a)



(b)



(c)

Figure 4: (a) A CT image of two containers, with the substrate in the left container receiving hydrocortisone two hours before being irradiated with the X-ray beam, and the substrate in the right container receiving no stimulus. (b) The substrate segment in the left container that is not directly exposed to stimuli. (c) The cortisol-exposed segment of the substrate in the left container.



Here,  $S$  is a discrete random variable that represents spike events, with potential outcomes in the set  $S = \{s_1, s_2, \dots, s_\eta\}$  and corresponding probabilities  $p_i \doteq \Pr(S = s_i)$  for  $i = 1, \dots, \eta$ .  $p_i$  is a discrete set of probabilities with the condition  $\sum_i p_i = 1$ , and  $q$  is the *entropic-index* or Rényi entropy order with  $q \geq 0$  and  $q \neq 1$ , which in our experiments was set to 2.

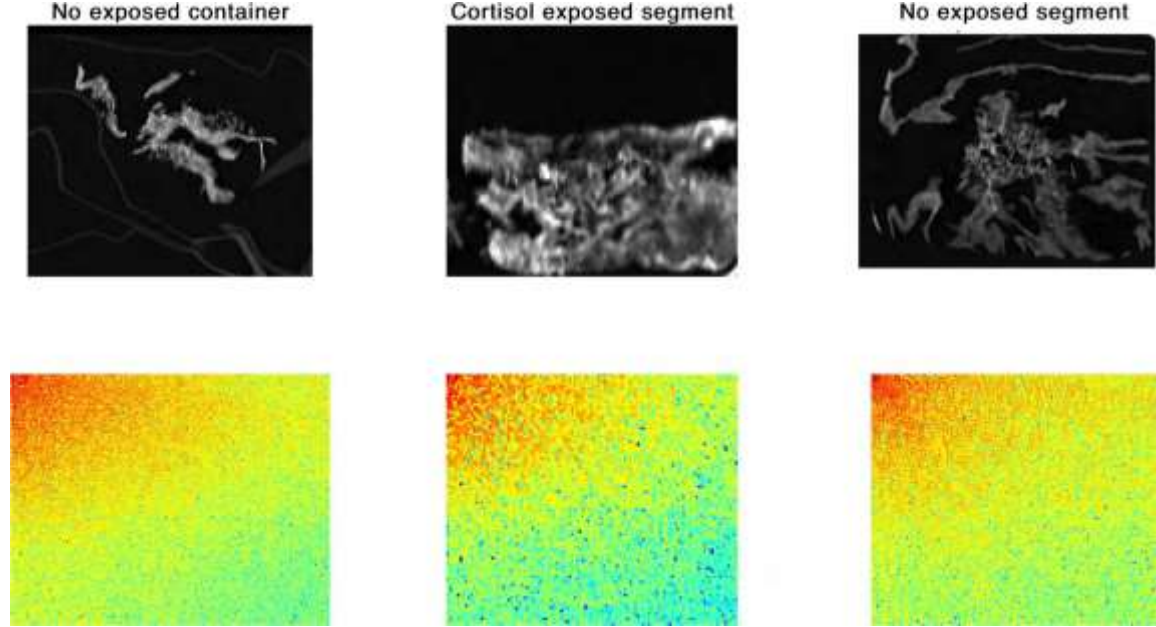


Figure 5: The results of applying DCT to CT images, where DCT expresses a finite sequence of data points as a sum of cosine functions oscillating at different frequencies. (a) On a non-exposed container, higher energies (red hue) are concentrated in the top left corner, while lower energies (green and blue hues) are concentrated in the bottom right corner. (b) The cortisol-exposed segment has a lower concentration of high energy in the top left corner and a higher dispersion of low energy (blue hue). (c) The no-exposed segment has a moderate energy distribution than the others, where the higher-energy spectral sub-bands are scattered rather than being concentrated in a few DCT coefficients.

We take the logarithm to be in base 2, since we interpreted the entire recording duration  $T$  with bits, with ‘1s’ indicating the availability of spike events and ‘0s’ otherwise. To determine spike diversity across all channels, we represent recordings by a binary matrix with a row for each channel. We calculated the Lempel–Ziv complexity ( $LZc$ ) over channels using the Kolmogorov complexity algorithm [30] to capture both temporal and spatial diversity. We then concatenated the rows of this binary matrix to form a single binary string and normalised  $LZc$  by dividing the raw value by the randomly shuffled value obtained for the same binary input sequence to obtain PCIPK. Since the value of PCIPK for a fixed-length binary sequence is maximum when it is totally random, the normalised values reflect the degree of signal diversity on a scale of 0 to 1.

Other metrics that were used to quantify the complexity of spike events are Simpson’s diversity, Space-filling, and Expressiveness. Simpson’s diversity is calculated as  $\Gamma = \sum_i (p(s_i))^{-2}$ . For  $H < 3$ , it correlates linearly with Shannon entropy, and the relationship becomes logarithmic for higher values of  $H$ . The value of  $\Gamma$  varies from 0 to 1, with 1 representing infinite diversity and 0 representing no diversity. Space-filling ( $\Delta$ ) is the ratio of non-zero entries in the binary representation of  $X$  to

Table 1: Qualitative description of electrical activity (1) 16 hours prior to hydrocortisone exposure and (2) 1 hour after hydrocortisone exposure.

Ch#	Spike#	Length (s)	Amplitude (V)	$H(\text{signal})$	$H(\text{spike})$	$\Gamma$	$\Delta$	Y	Kolmogorov	PCIpK	$T_q$	$R_q$
16 hours prior to the trigger event												
1	455	2.91	-1.20	-3.40	242.2	0.99	0.0078	$3.07 \times 10^1$	0.055	$3.86 \times 10^{-03}$	-3.230	-0.62
2	449	2.76	-0.32	-3.72	239.6	0.99	0.0077	$3.07 \times 10^1$	0.052	$3.64 \times 10^{-03}$	-2.498	-0.29
3	457	2.72	-0.02	-3.88	243.1	0.99	0.0079	$3.06 \times 10^1$	0.053	$3.66 \times 10^{-03}$	-0.001	12.52
4	449	3.40	-3.58	-3.74	239.6	0.99	0.0077	$3.07 \times 10^1$	0.052	$3.73 \times 10^{-03}$	-46.884	-3.70
5	460	2.23	1.18	-3.43	244.5	0.99	0.0079	$3.06 \times 10^1$	0.055	$3.64 \times 10^{-03}$	0.002	12.27
6	446	3.19	-1.09	-3.26	238.3	0.99	0.0077	$3.08 \times 10^1$	0.052	$3.69 \times 10^{-03}$	-6.544	-1.49
7	464	2.73	0.26	-3.58	246.2	0.99	0.0080	$3.06 \times 10^1$	0.054	$3.59 \times 10^{-03}$	0.102	4.30
1 hour after the trigger event												
1	29	2.38	-1.08	-5.72	20.60	0.96	0.0080	$2.55 \times 10^3$	0.062	0.048	-3.68	-0.78
2	28	2.97	-0.80	-5.49	20.01	0.96	0.0077	$2.57 \times 10^3$	0.062	0.047	-1.93	0.04
3	30	2.52	-0.14	-5.38	21.18	0.96	0.0083	$2.54 \times 10^3$	0.065	0.047	-0.12	4.43
4	27	3.15	-6.15	-5.56	19.41	0.96	0.0075	$2.58 \times 10^3$	0.065	0.051	-47.67	-3.71
5	28	1.41	-0.22	-5.73	20.01	0.96	0.0077	$2.57 \times 10^3$	0.062	0.045	-0.10	4.64
6	32	2.42	-2.43	-5.70	22.34	0.96	0.0088	$2.51 \times 10^3$	0.075	0.049	-8.47	-1.79
7	29	2.03	0.25	-5.51	20.60	0.96	0.0080	$2.55 \times 10^3$	0.068	0.050	0.23	1.83

the total duration of the recording  $T$ . Expressiveness (Y) is calculated as the Shannon entropy  $H$  divided by space-filling ratio  $\Delta$ , which represents the economy of diversity.

### 3. Results

Table 1 presents a qualitative description of electrical activity for one of the trials, where all complexity metrics can be compared for the condition in which the substrate was exposed 16 hours before hydrocortisone exposure and 1 hour after hydrocortisone exposure.

Figure 6 graphically summarises the qualitative description of electrical activity for all trials in a multi-curve layout that can be used to easily identify those metrics that are more influenced by stimulation with hydrocortisone and can thus be used to track the impacts in electrical dynamics complexity. The different panels implicitly represent time, where Fig. 6(a) refers to 16 hours before exposure, Fig. 6(b) refers to the exposure or trigger event, and Fig. 6(c) refers to 1 hour after exposure. The x-axis, where the channels are aligned, represents space. Those complexity metrics with no variation appear flat (for example after trigger the Shannon entropy for the signal, shown in red in the plots). Those influenced show positive or negative peaks, either to the left (Shannon entropy for the spike event, Simpson's diversity, Space-filling, Expressiveness, Kolmogorov Complexity, and PCIpK) or towards the right of the sample (Tsallis and Rényi entropies). By superimposing complexity metrics on each channel and reconstructing the time evolution of the spiking dynamics the mycelium, we can create a graphical representation of the excitatory or inhibitory state before, during, and after hydrocortisone exposure, demonstrating the formation of an electrical activity fingerprint that corresponds to that specific event (see Fig. 6(e)).

We found that the PCIpK, Tsallis, and Rényi entropies are the most relevant metrics for system analysis among all complexity measurements considered here (see Fig. 7). The PCIpK measure provides an easy inspection of the substrate's evolution analysis, including its spatio-temporal features. Figure 7(a) shows that a hydrocortisone stimulus induces a much stronger response in the application locus. Following a stimulus, some excitation events can be seen propagating in the substrate at much lower potentials. Tsallis entropy, as shown in Fig. 7(b), is less sensitive but more accurate in tracking the evolution of the reference electrode signal. We can see from Fig. 7(c) that Rényi entropy helps us to monitor peak evolution over time.

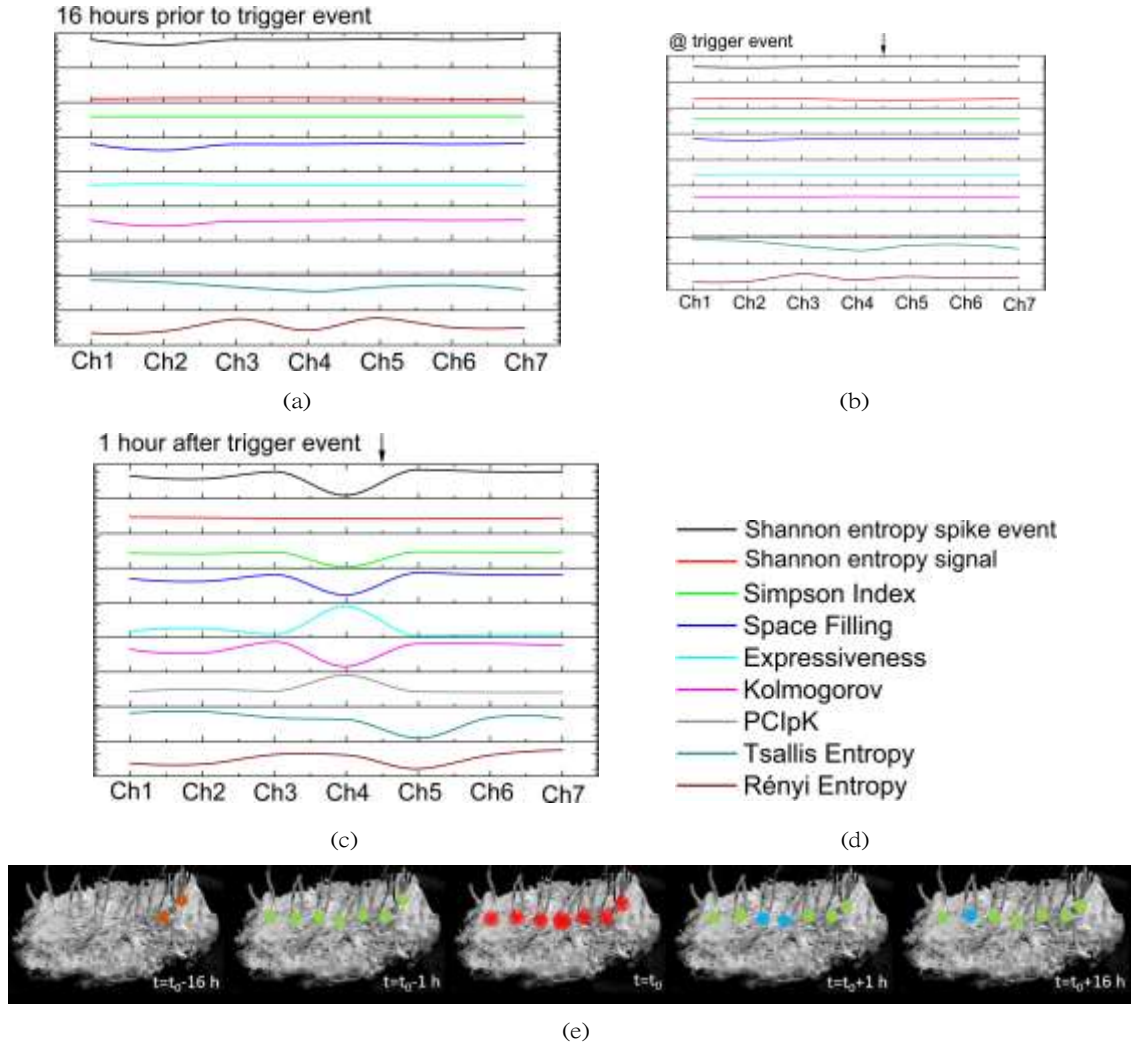


Figure 6: (a) Evolution related to a data segment recorded 16 hours before hydrocortisone exposure. (b) Cortisol-exposed data segment (trigger event). (c) Evolution related to a data segment recorded 1 hour after hydrocortisone exposure. (d) Merit figures of complexity measures performed on recorded potentials, legend. (e) Graphical representation of the living substrate with measurement electrodes and PCIPK complexity defined by a colour code (light blue  $< 0.5$ ,  $0.5 < \text{green} < 0$ ,  $0 < \text{orange} < 0.5$ , red  $> 0.5$ ). In the inset, the reference time of each frame is specified.

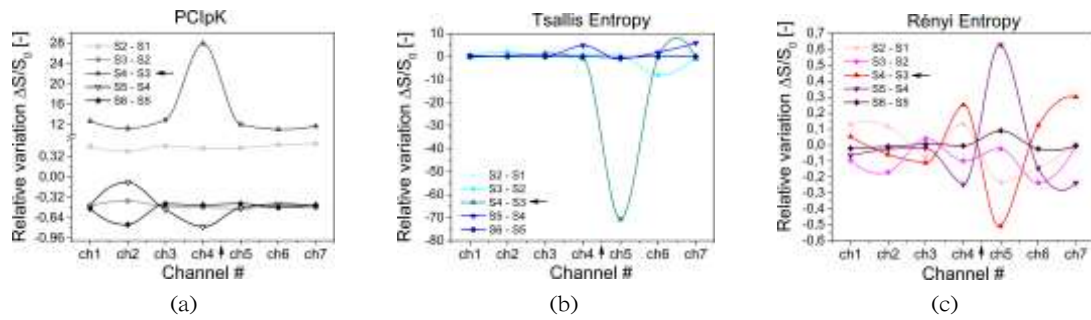


Figure 7: (a) PCIpK is measured as a function of the measurement segments (which are time-dependent), with the arrows indicating both the spatial locus for hydrocortisone stimulation and the temporal segment corresponding to the trigger. The time interval used to compute the relative variance is denoted by  $S(n + 1) - S(n)$ . (b) Tsallis Entropy. (c) Rényi Entropy.

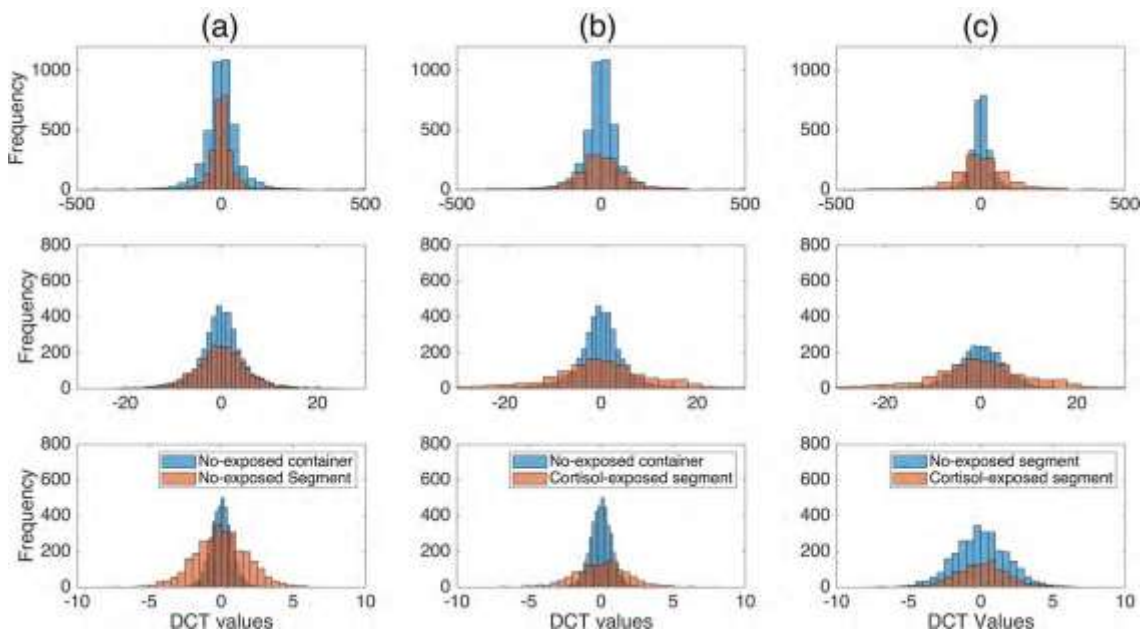


Figure 8: The comparison of the distribution of energy levels in the calculated DCT for (a) no-exposed container and no-exposed segment, (b) no-exposed container and cortisol-exposed segment, and (c) no-exposed segment and cortisol-exposed segment. The substrate that was not exposed to hydrocortisone had a higher energy frequency than the cortisol-exposed segment and the no-exposed segment adjacent to the cortisol-exposed segment.

### 3.1. Internal inspection of the fungal culture

The visual appearance of the substrates colonised by the fungi did not change after exposure to hydrocortisone. However, the impact of hydrocortisone exposure is visible in the distribution of energy levels as a result of applying DCT to CT images, as shown in Fig. 8. The calculated DCT values for no-exposed container, no-exposed segment, and cortisol-exposed segment were divided into three parts, including the distribution of values for high, medium, and low energies, which are shown in the first, middle, and last rows, respectively. The substrate that was not exposed to hydrocortisone had a higher energy frequency than the cortisol-exposed segment and the no-exposed segment adjacent to the cortisol-exposed segment.

## 4. Discussion

The integrity of the fungal colony is preserved by cytoplasm flow in the mycelium network, where calcium waves [24] change the flow's propagation coordination. Cortisol metabolism stimulates the production of receptor activator of nuclear factor-kappa-B ligand (RANKL), a type II membrane protein that regulates bone regeneration and remodelling in mammals [31]. The activity of cells responsible for calcium resorption from bone is inhibited when RANKL is stimulated [32]. The elevated circulating cortisol levels maintain stress levels, triggering physiological changes in the body's regulatory networks. Hog1 is a stress-activated mitogen-activated protein kinase (MAPK) in fungi that is homologous to the p38 MAPK pathways in mammals [33]. When exposed to stress conditions, Hog1 rapidly dephosphorylates and induces the appropriate cellular responses against the offending environmental stimuli [34]. We speculate that receiving cortisol by the substrate can inhibit the flow of calcium and, in turn, reduce its physiological changes.

## 5. Conclusion

We conclude that the effects of hydrocortisone exposure on a *Pleurotus ostreatus* mycelium can be demonstrated using a well-known combination of techniques in a proper interdisciplinary approach. The computed tomography shows a change in grey tones as a result of hydrocortisone exposure, which is associated with active ion transport triggered in the living mycelium in response to the hormone. Simultaneously, by capturing biopotential signals and extracting their numerical complexity, we could identify consistent metrics for tracing the stimulus and tracking the propagation of ionic waves in response to the hormone. Our research extends our understanding of living fungal, which could be used in future wearable and architectural systems to benefit living species while also maximising sustainability.

## Acknowledgement

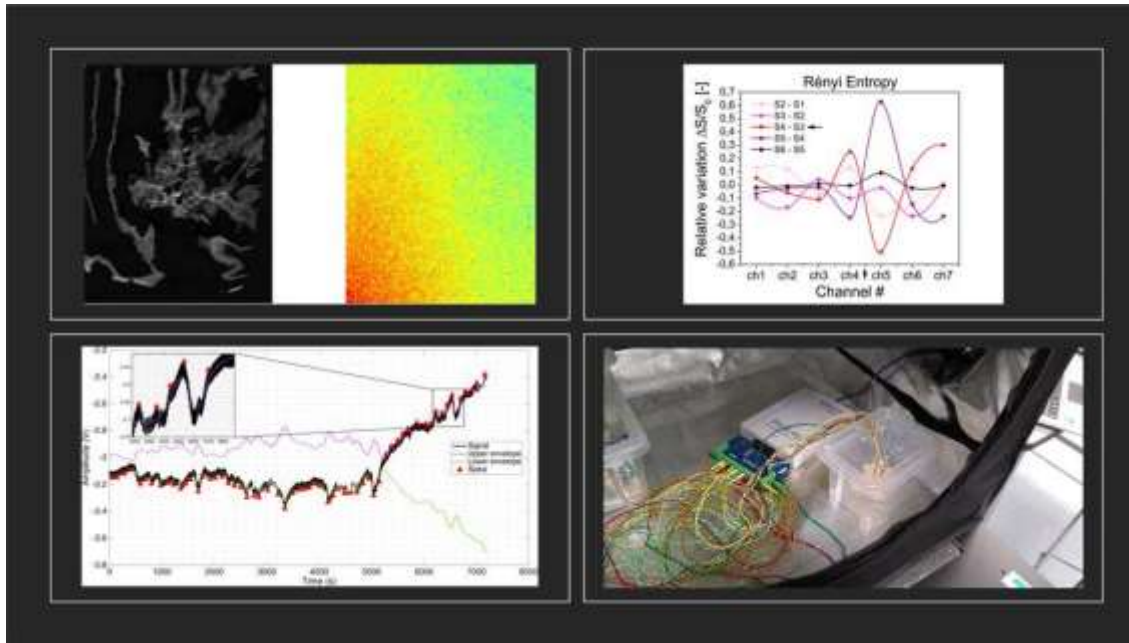
This project has received funding from the European Union's Horizon 2020 research and innovation programme FET OPEN "Challenging current thinking" under grant agreement No 858132.

The authors would like to thank Vasilis Mitsios and Stamatis Varvanikolakis for coordinating the scans at Bioiatriki, as well as Judith Gómez Cuyàs for her constructive suggestion.

**For Table of Contents Use Only**

**Manuscript title:** On stimulating fungi *Pleurotus ostreatus* with Hydrocortisone

**Authors:** Mohammad Mahdi Dehshibi, Alessandro Chiolerio, Anna Nikolaidou, Richard Mayne, Antoni Gandia, Mona Ashtari, Andrew Adamatzky



## References

- [1] F. Cottier, F. A. Mühlshlegel, Communication in fungi, *International journal of microbiology* 2012 (2012) 1–9.
- [2] R. Alonso-Monge, E. Román, D. Arana, J. Pla, C. Nombela, Fungi sensing environmental stress, *Clinical Microbiology and Infection* 15 (2009) 17–19.
- [3] L. Hou, L. Wang, X. Wu, W. Gao, J. Zhang, C. Huang, Expression patterns of two pal genes of *pleurotus ostreatus* across developmental stages and under heat stress, *BMC microbiology* 19 (2019) 1–16.
- [4] A. Adamatzky, On spiking behaviour of oyster fungi *pleurotus djamor*, *Scientific reports* 8 (2018) 1–7.
- [5] A. E. Beasley, A. L. Powell, A. Adamatzky, Capacitive storage in mycelium substrate, arXiv preprint arXiv:2003.07816 (2020).
- [6] A. E. Beasley, A. L. Powell, A. Adamatzky, Fungal photosensors, arXiv preprint arXiv:2003.07825 (2020).
- [7] A. Adamatzky, A. Chiolerio, G. Sirakoulis, Electrical resistive spiking of fungi, *Biophysical Reviews and Letters* 16 (2021) 1–7.
- [8] A. Adamatzky, Towards fungal computer, *Interface focus* 8 (2018) 20180029.
- [9] A. Adamatzky, E. Goles, G. J. Martinez, M.-A. Tsompanas, M. Tegelaar, H. A. Wosten, Fungal automata, *Complex Systems* 29 (2020) 759–778.
- [10] M. M. Dehshibi, A. Adamatzky, Electrical activity of fungi: Spikes detection and complexity analysis, *Biosystems* 203 (2021) 104373.
- [11] A. Adamatzky, P. Ayres, G. Belotti, H. Wösten, Fungal architecture position paper, *International Journal of Unconventional Computing* 14 (2019).
- [12] A. Adamatzky, M. Tegelaar, H. A. Wosten, A. L. Powell, A. E. Beasley, R. Mayne, On boolean gates in fungal colony, *Biosystems* 193 (2020) 104138.
- [13] E. Goles, M.-A. Tsompanas, A. Adamatzky, M. Tegelaar, H. A. Wosten, G. J. Martínez, Computational universality of fungal sandpile automata, *Physics Letters A* 384 (2020) 126541.
- [14] A. Adamatzky, A. Gandia, A. Chiolerio, Towards fungal sensing skin, *Fungal Biology and Biotechnology* 8 (2021) 1–7.
- [15] A. Adamatzky, A. Nikolaidou, A. Gandia, A. Chiolerio, M. M. Dehshibi, Reactive fungal wearable, *Biosystems* 199 (2021) 104304.
- [16] H.-J. Jang, T. Lee, J. Song, L. Russell, H. Li, J. Dailey, P. C. Searson, H. E. Katz, Electronic cortisol detection using an antibody-embedded polymer coupled to a field-effect transistor, *ACS applied materials & interfaces* 10 (2018) 16233–16237.

- [17] A. Kaushik, A. Vasudev, S. K. Arya, S. K. Pasha, S. Bhansali, Recent advances in cortisol sensing technologies for point-of-care application, *Biosensors and Bioelectronics* 53 (2014) 499–512.
- [18] E. Russell, G. Koren, M. Rieder, S. H. Van Uum, The detection of cortisol in human sweat: implications for measurement of cortisol in hair, *Therapeutic drug monitoring* 36 (2014) 30–34.
- [19] N. Gholami, M. M. Dehshibi, A. Adamatzky, A. Rueda-Toicen, H. Zenil, M. Fazlali, D. Masip, A novel method for reconstructing ct images in gate/geant4 with application in medical imaging: A complexity analysis approach, *Journal of Information Processing* 28 (2020) 161–168.
- [20] L. Marple, Computing the discrete-time “analytic” signal via fft, *IEEE Transactions on signal processing* 47 (1999) 2600–2603.
- [21] C. E. Shannon, Communication in the presence of noise, *Proceedings of the IRE* 37 (1949) 10–21.
- [22] F. M. Dekking, C. Kraaikamp, H. P. Lopuhaä, L. E. Meester, *A Modern Introduction to Probability and Statistics: Understanding why and how*, Springer Science & Business Media, 2005. doi:10.1007/1-84628-168-7.
- [23] P. Barca, M. Giannelli, M. E. Fantacci, D. Caramella, Computed tomography imaging with the adaptive statistical iterative reconstruction (asir) algorithm: dependence of image quality on the blending level of reconstruction, *Australasian physical & engineering sciences in medicine* 41 (2018) 463–473.
- [24] J. Aramburu, J. Heitman, G. R. Crabtree, Calcineurin: a central controller of signalling in eukaryotes: Workshop on the calcium/calcineurin/nfat pathway: Regulation and function, *EMBO reports* 5 (2004) 343–348.
- [25] J. Fan, M. Farmen, I. Gijbels, Local maximum likelihood estimation and inference, *Journal of the Royal Statistical Society: Series B (Statistical Methodology)* 60 (1998) 591–608.
- [26] D. Petz, *Quantum information theory and quantum statistics*, Springer Science & Business Media, 2007. doi:10.1007/978-3-540-74636-2.
- [27] C. E. Shannon, A mathematical theory of communication, *The Bell system technical journal* 27 (1948) 379–423.
- [28] A. Rényi, On measures of entropy and information, in: *Proceedings of the Fourth Berkeley Symposium on Mathematical Statistics and Probability, Volume 1: Contributions to the Theory of Statistics*, University of California Press, 1961, pp. 547–561.
- [29] C. Tsallis, Possible generalization of boltzmann-gibbs statistics, *Journal of statistical physics* 52 (1988) 479–487.
- [30] F. Kaspar, H. Schuster, Easily calculable measure for the complexity of spatiotemporal patterns, *Physical Review A* 36 (1987) 842.
- [31] Y. S. Chyun, B. E. Kream, L. G. Raisz, Cortisol decreases bone formation by inhibiting periosteal cell proliferation, *Endocrinology* 114 (1984) 477–480.



- [32] E. Davies, C. Kenyon, R. Fraser, The role of calcium ions in the mechanism of acth stimulation of cortisol synthesis, *Steroids* 45 (1985) 551–560.
- [33] S. Hohmann, Osmotic stress signaling and osmoadaptation in yeasts, *Microbiology and molecular biology reviews* 66 (2002) 300–372.
- [34] Y.-S. Bahn, K. Kojima, G. M. Cox, J. Heitman, Specialization of the hog pathway and its impact on differentiation and virulence of *cryptococcus neoformans*, *Molecular biology of the cell* 16 (2005) 2285–2300.